

# Space environment of Mercury at the time of the first MESSENGER flyby: Solar wind and interplanetary magnetic field modeling of upstream conditions

Daniel N. Baker,<sup>1</sup> Dusan Odstroil,<sup>2,3</sup> Brian J. Anderson,<sup>4</sup> C. Nick Arge,<sup>5</sup> Mehdi Benna,<sup>6</sup> George Gloeckler,<sup>7</sup> Jim M. Raines,<sup>7</sup> David Schriver,<sup>8</sup> James A. Slavin,<sup>9</sup> Sean C. Solomon,<sup>10</sup> Rosemary M. Killen,<sup>11</sup> and Thomas H. Zurbuchen<sup>7</sup>

Received 23 March 2009; revised 7 July 2009; accepted 20 July 2009; published 2 October 2009.

[1] The first flyby of Mercury by the Mercury Surface, Space Environment, Geochemistry and Ranging (MESSENGER) spacecraft occurred on 14 January 2008. In order to provide contextual information about the solar wind (SW) properties and the interplanetary magnetic field near the planet, we have used an empirical modeling technique combined with a numerical physics-based SW model. The Wang-Sheeley-Arge (WSA) method uses solar photospheric magnetic field observations (from Earth-based instruments) in order to estimate inner heliospheric conditions out to 21.5 solar radii from the Sun. This information is then used as input to the global numerical magnetohydrodynamic model, ENLIL, which calculates SW velocity, density, temperature, and magnetic field strength and polarity throughout the inner heliosphere. The present paper shows WSA-ENLIL conditions computed for the several week period encompassing the first flyby. This information is used in conjunction with MESSENGER magnetometer data (and the only limited available MESSENGER SW plasma data) to help understand the Mercury flyby results. The in situ spacecraft data, in turn, can also be used iteratively to improve the model accuracy for inner heliospheric “space weather” purposes. Looking to the future, we discuss how with such modeling we can estimate relatively continuously the SW properties near Mercury and at the cruise location of MESSENGER now, for upcoming flybys, and toward the time of spacecraft orbit insertion in 2011.

**Citation:** Baker, D. N., et al. (2009), Space environment of Mercury at the time of the first MESSENGER flyby: Solar wind and interplanetary magnetic field modeling of upstream conditions, *J. Geophys. Res.*, 114, A10101, doi:10.1029/2009JA014287.

## 1. Introduction

[2] The Mercury Surface, Space Environment, Geochemistry, and Ranging (MESSENGER) spacecraft was launched on 3 August 2004. The spacecraft then began its long, circuitous route toward eventual insertion into Mercury orbit in March 2011. MESSENGER had two flybys of Venus (October 2006 and June 2007) and, on 14 January 2008, had its first of three flybys of Mercury. This successful

initial transit through the near environs of Mercury [Solomon *et al.*, 2008] gave the first close views of the Mercury surface, atmosphere, and magnetosphere since the Mariner 10 flybys of 1974 and 1975 [e.g., Russell *et al.*, 1988].

[3] During the period around MESSENGER’s closest approach to the planet, which occurred at ~1905 UTC on 14 January, the magnetometer and the Energetic Particle and Plasma Spectrometer (EPPS) recorded a variety of interesting magnetospheric phenomena [Slavin *et al.*, 2008]. However, the in situ measurements, as well as the inferences from measurements made prior to and following the magnetospheric passage, suggested that the solar wind (SW) and interplanetary magnetic field (IMF) *B* during the particular

<sup>1</sup>Laboratory for Atmospheric and Space Physics, University of Colorado at Boulder, Boulder, Colorado, USA.

<sup>2</sup>National Oceanic and Atmospheric Administration, Boulder, Colorado, USA.

<sup>3</sup>Also at Cooperative Institute for Research in Environmental Sciences, University of Colorado at Boulder, Boulder, Colorado, USA.

<sup>4</sup>Johns Hopkins University Applied Physics Laboratory, Laurel, Maryland, USA.

<sup>5</sup>Air Force Research Laboratory, Kirtland Air Force Base, New Mexico, USA.

<sup>6</sup>Solar System Exploration Division, NASA Goddard Space Flight Center, Greenbelt, Maryland, USA.

<sup>7</sup>Department of Atmospheric, Oceanic and Space Sciences, University of Michigan, Ann Arbor, Michigan, USA.

<sup>8</sup>Institute for Geophysics and Planetary Physics, University of California, Los Angeles, California, USA.

<sup>9</sup>Heliophysics Science Division, NASA Goddard Space Flight Center, Greenbelt, Maryland, USA.

<sup>10</sup>Department of Terrestrial Magnetism, Carnegie Institution of Washington, Washington, D. C., USA.

<sup>11</sup>Department of Astronomy, University of Maryland, College Park, Maryland, USA.

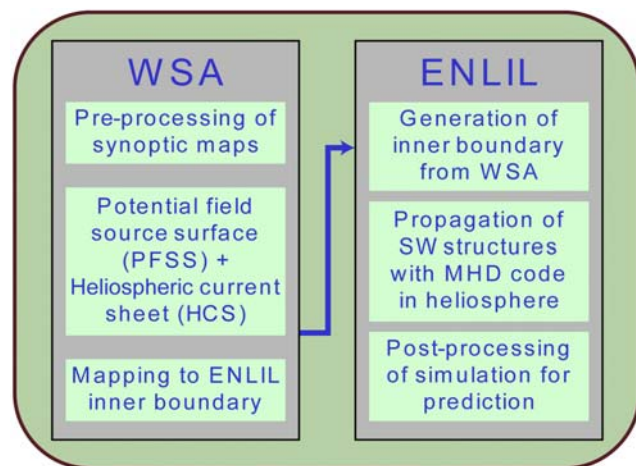


**Figure 1.** Elements of the real-time coupled coronal-heliospheric model used in the present study. GONG data are used as input for the synoptic maps, and forecast outputs are given at the test bed site (<http://Helios.swpc.noaa.gov/enlil/latest-velocity.html>). Definitions and abbreviations are described in the text.

time of the flyby were not very conducive to strong magnetospheric substorm or particle acceleration events of the type seen by Mariner 10 instruments [e.g., Baker *et al.*, 1986] due to the fact the IMF was northward throughout the passage.

[4] The limitations of having measurements of the inner heliospheric SW and IMF conditions at only a single location have made it evident that a broader contextual view of the Mercury (and MESSENGER) space environment is valuable. For example, it is useful to know about large-scale and medium-scale interplanetary structures that may be present near MESSENGER, such as high-speed SW streams, corotating interaction regions, and IMF polarity reversal boundaries. Present-day solar observations (made from Earth-based facilities), along with empirical and physics-based models, have the potential to provide a good global picture of the inner heliosphere [Arge *et al.*, 2004; Owens *et al.*, 2005].

[5] In this paper, we first describe current state-of-the-art modeling techniques. We then show the application of these techniques to the MESSENGER flyby period in order to place the spacecraft results into a broad physical perspective. We make specific comparisons of the model results with measurements at 1 AU and also from the relevant MESSENGER sensors before and after the planetary encounter. We conclude with a general discussion of a strategy for using our modeling approaches for future MESSENGER and other (remote) Mercury observations.

## 2. Modeling Inner Heliospheric Properties

[6] The Wang-Sheeley-Argé (WSA) model is a combined empirical and physics-based representation of the quasi-steady global SW flow [Arge *et al.*, 2004]. It has been used in prior work to predict the ambient SW speed and IMF polarity at Earth (as well as other points in the inner heliosphere) and is an extension of the original Wang and Sheeley model [Wang and Sheeley, 1992]. The model uses

ground-based observations of the Sun’s surface magnetic field as input to a magnetostatic potential field source surface model [Schatten *et al.*, 1969] of the coronal field (see Figure 1). The effects of outward flows in the corona, which are not explicitly contained in the formulation, are approximated by the imposition of radial field boundary conditions at the source surface, which is a Sun-centered sphere typically positioned at  $2.5 R_S$ , where  $R_S$  is the solar radius. A number of important changes have been made to the Wang-Sheeley model [Arge and Pizzo, 2000], including (1) improvements to the model inputs, which are the line of sight (LOS) photospheric magnetic fields, and (2) improvements to the empirical kinematic model itself.

[7] The photospheric field observations are the basic large-scale observable used to drive the computations and serve as a key input to all coronal and SW models. Here we use updated photospheric field synoptic maps (i.e., synoptic maps updated four times a day with new magnetograms) constructed with LOS magnetograms from the National Solar Observatory’s Global Oscillation Network Group (GONG) system. These ground-based data provide the present “standard” data input for WSA modeling. Because observational evidence suggests that the solar magnetic field is nearly radial at the photosphere (except in strong active regions), the LOS field measurements from these data sources have been converted to radial [see Arge *et al.*, 2004].

[8] Using WSA results relatively near the Sun, an ideal magnetohydrodynamic simulation called ENLIL [Odstrcil *et al.*, 2004; Tóth and Odstrcil, 1996] is then performed to model the SW flow outward to beyond 1 AU. The computational domain is the uniform grid occupying the sector of a sphere defined by pairs of boundaries at fixed radii (inner and outer), at fixed meridional angles (north and south), and at fixed azimuthal angles (east and west). The position of the inner boundary is set at 0.1 AU ( $\approx 21.5 R_S$ ), and the outer boundary is set at 1.1 AU. The meridional and azimuthal extents span  $30\text{--}150^\circ$  and  $0\text{--}360^\circ$ , respectively. The inner boundary lies in the supersonic flow region, near the outer field of view of the Large Angle and Spectrometric Coronagraph C3 on the Solar Heliospheric Observatory spacecraft. The outer boundary is chosen to enable recording of simulated temporal profiles of SW properties at and near the Earth position [Odstrcil *et al.*, 2004].

## 3. Mercury Flyby: Modeled Inner Heliosphere Conditions

[9] The product of the combined WSA-ENLIL modeling is a specification of the SW flow speed, plasma density, SW plasma temperature, and magnetic field strength throughout the inner part of the heliosphere. Prior modeling work has tended to focus on optimization of modeled results near the Earth’s location at 1 AU, or at the first Lagrangian point, L1, which is the location of the Advanced Composition Explorer (ACE) spacecraft. New data now available from the dual spacecraft Solar Terrestrial Relations Observatory (STEREO) mission have provided a very useful broader range of SW measurements with which to compare WSA-ENLIL results (see <http://stereo.gsfc.nasa.gov>).

[10] A color representation of the radial flow speed ( $V_r$ ) in the equatorial plane computed for the entire inner heliosphere

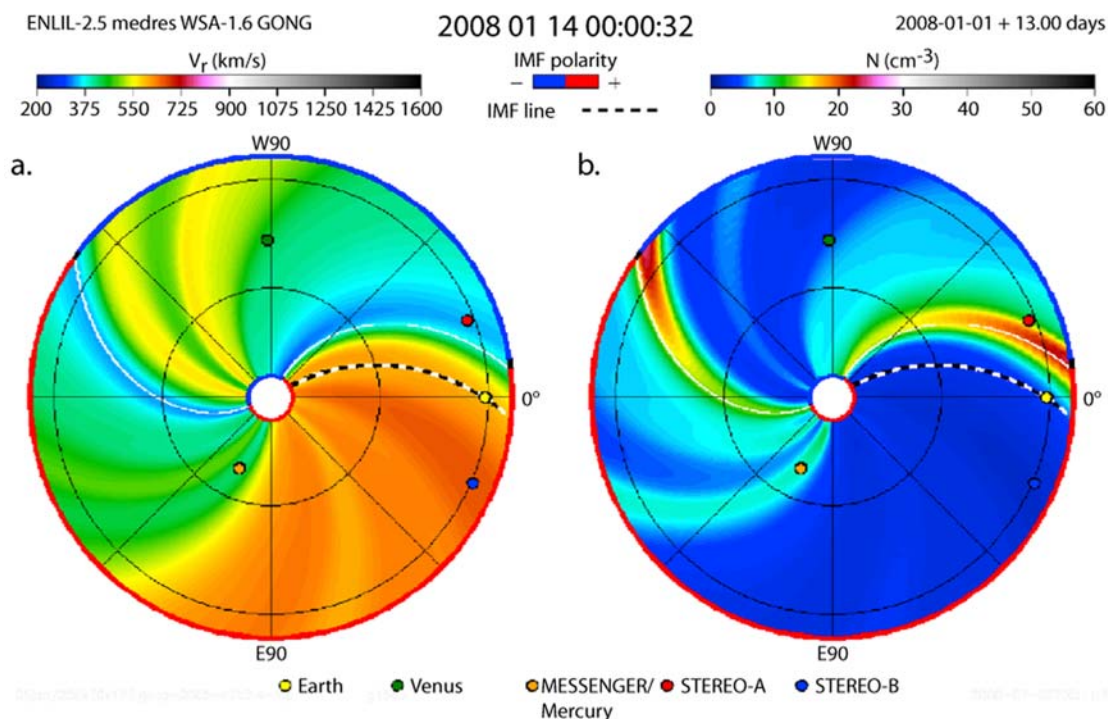


**Figure 2.** (a) Modeled radial SW speed and (b) density in the equatorial plane, viewed from the north ecliptic pole, obtained from the WSA-ENLIL model near the time of the first MESSENGER flyby of Mercury. The color scale for  $V_r$  is given by the color bar above Figure 2a. As shown at the bottom, the locations of Earth, STEREO-A, STEREO-B, Venus, Mercury, and the MESSENGER spacecraft are all indicated by small colored dots. The inner domain of the model (where WSA is utilized) is denoted by the white central circle. The computational domain of the ENLIL simulation is shown by the colored area. A nominal computed magnetic field line is indicated by the heavy dashed line extending from the inner boundary outward through the Earth past 1 AU. The red-blue color coding along the edge of the outer boundary shows the polarity of the IMF: red indicates IMF positive, or pointing away from the Sun, while blue indicates negative polarity with the IMF pointing toward the Sun. The white curves mark the estimated IMF polarity sector boundaries in the equatorial plane. The SW density in the inner heliosphere modeled by WSA-ENLIL and shown in Figure 2b is scaled by  $r^2$  to the value at 1 AU.

early on 14 January 2008 is shown in Figure 2a. From the model results, we see that a well-developed broad SW stream region was expected in the heliosphere during this time. The prominent modeled SW speed enhancement (up to  $\sim 600$  km/s) at  $\sim 1$  AU was in the approximate longitude sector  $-135$ – $0^\circ$  (mostly behind the azimuthal location of the Earth), where  $0^\circ$  is the direction toward Earth. According to the model, the stream would have enveloped STEREO-B at the time of the snapshot but had not yet reached STEREO-A (see section 3.1 and Figures 3–5 for detailed model-data comparison). MESSENGER and Mercury, of course, were effectively collocated at the time of the snapshot and were subjected to essentially identical SW flow conditions. From a Mercury magnetospheric response perspective, there was no significant SW speed enhancement expected to be seen near the planet on the particular day of the spacecraft flyby. The high-speed stream under discussion would have passed over the planet (and MESSENGER) several days prior to the flyby of Mercury with the highest-speed (600 km/s) stream features having been expected to rotate over the Mercury location some 10–11 days earlier. Benign SW

conditions at Mercury on  $\sim 14$  January (as suggested by the model) meant that the magnetosphere was relatively quiescent during the spacecraft passage, as was observed [Slavin *et al.*, 2008].

[11] Another important control on Mercury's magnetospheric configuration and physical extent is the density ( $N$ ) of the incident SW. Higher density along with higher flow speeds would imply higher SW dynamic pressure ( $P_{\text{dyn}} = mNV^2$ , where  $m$  is the effective SW ion mass and  $V$  is the scalar flow speed) and also could suggest higher impacts of SW particles onto the magnetic polar regions of Mercury's surface [see McClintock *et al.*, 2008]. The WSA-ENLIL model is able to provide global modeling estimates of SW density throughout the inner heliosphere for the same modeling domain (as was shown above for SW speed).

[12] Color-coded density computation results for 14 January 2008 are shown in Figure 2b. From Figure 2b, it is seen that two relatively high-density regions of SW plasma were expected from this model. One lay ahead (between  $0$  and  $\sim 45^\circ$  ecliptic longitude at 1 AU) of the high-speed SW stream shown in Figure 2a and bracketed

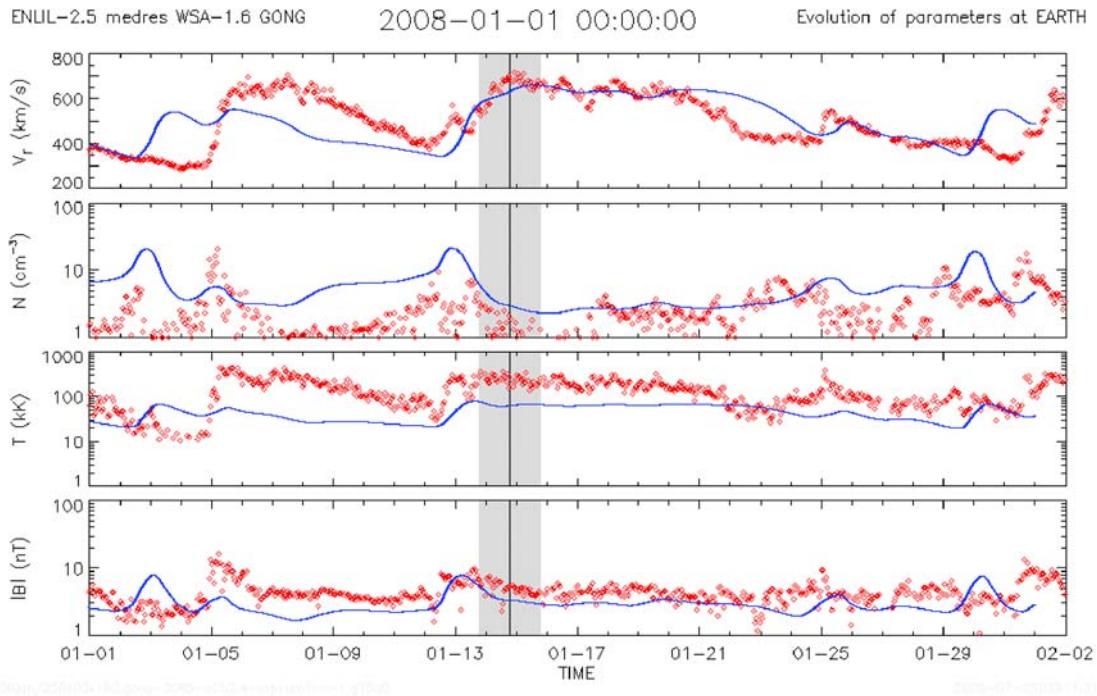


**Figure 3.** ACE measurements of (first panel) SW speed, (second panel) density, and (third panel) plasma temperature and (fourth panel) IMF magnitude, all as 1-h averages measured at the upstream Lagrangian (L1) point, are shown by the red traces for 1–31 January 2008. The smooth blue curves show WSA-ENLIL model values for the same period. The 48 h bracketing the first MESSENGER flyby of Mercury (vertical line) are shaded.

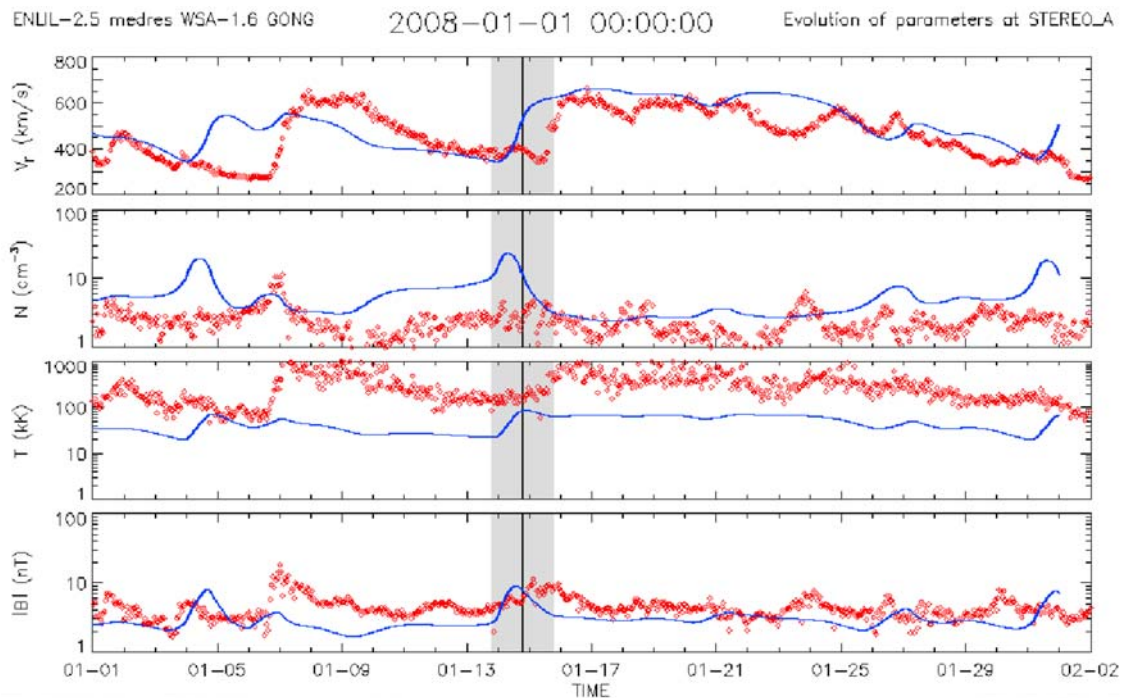


**Figure 4.** Similar to Figure 3 but for the STEREO-A spacecraft near 1 AU at solar longitude ahead of the Earth's position (as described in the text).

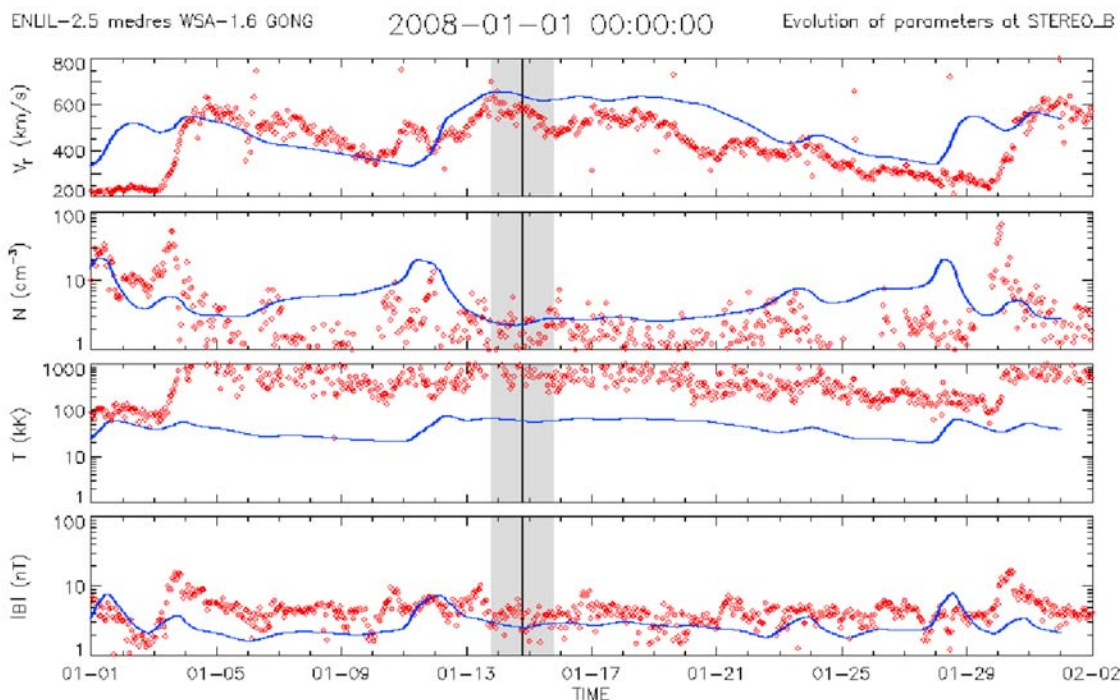


**Figure 5.** Similar to Figure 3 but for the STEREO-B spacecraft near 1 AU at solar longitude behind the Earth’s position (as described in the text).

the IMF polarity reversal boundary (shown by the white spiral curve in Figure 2b). This density enhancement was modeled to be greatest near 1 AU, but it extended all the way inward to the inner boundary of the ENLIL computation.

[13] A second modeled high-density region is seen in Figure 2b to bracket the other IMF polarity reversal region in the longitude sector from  $135^\circ$  to  $\sim 150^\circ$  at 1 AU. The boundary of a third slightly increased density region was seen in the model calculations to extend over the location of Mercury and MESSENGER at the time of this snapshot. However, this density stream was much weaker than the other two that were in other sectors of the inner heliosphere.

#### 4. Comparison of Model Results With Data at 1 AU

[14] As noted in section 3, WSA-ENLIL modeling results have been used extensively to “forecast” the SW and IMF values at 1 AU using ground-based solar input data (e.g., from the GONG network). In principle, such modeling results can give 3–4 day forecasts of SW properties [e.g., Baker *et al.*, 2004]. The model results can be readily compared with real-time measurements from such spacecraft missions as ACE and STEREO.

[15] The period of January 2008 was characterized by two broad SW streams (see Figure 2) that were persistent and well developed throughout the inner heliosphere (Figure 3). ACE observations for that period show the onset of a high-speed stream on 5 January, with a large-density spike just at the leading edge of the fast stream. Another high-speed stream commenced on about 13 January with a weaker density enhancement at the leading edge of this stream as well. This second stream persisted broadly for over a week

at ACE, and the SW speed eventually diminished to about 400 km/s by  $\sim 23$  January.

[16] The WSA-ENLIL modeling results for this interval of time are shown by the smooth blue lines in each panel of Figure 3. It is seen that most of the general features of the SW properties were seen similarly in the model. Certainly the two SW streams were clearly simulated by the model. The second stream (13–21 January) is very well fit both in time profile and in actual SW speed. During this period, the density, temperature, and magnetic field strength values all are also matched well by the model. The first stream (5–11 January) is less well fit than the second stream. It is seen that the modeled SW speed rises too late (by about 1 day), and the other parameters ( $N$ ,  $T$ , and  $B$ ) are also modeled to rise a bit late, and absolute values are not fit as accurately as they are for the second stream event.

[17] It is interesting to compare and contrast model results with data from other platforms near 1 AU for this same period. We show in Figures 4 and 5 the measurements at STEREO-A and STEREO-B that are comparable to the measurements from ACE in Figure 3. (The relative positions of the STEREO spacecraft are shown in Figure 2). Because of the general physical proximity of the STEREO-A and STEREO-B spacecraft to ACE, we see most of the SW stream features at all three spacecraft. However, substantial timing differences are seen at the three locations.

[18] We emphasize that correct characterization of the solar wind stream properties at the three separated spatial locations (ACE, STEREO-A, and STEREO-B) is an important validation of the model’s capabilities. Getting the arrival times correct at the three disparate solar longitudes indicates that the solar wind stream, indeed, has the essential structure predicted by the model and shown in Figure 2.

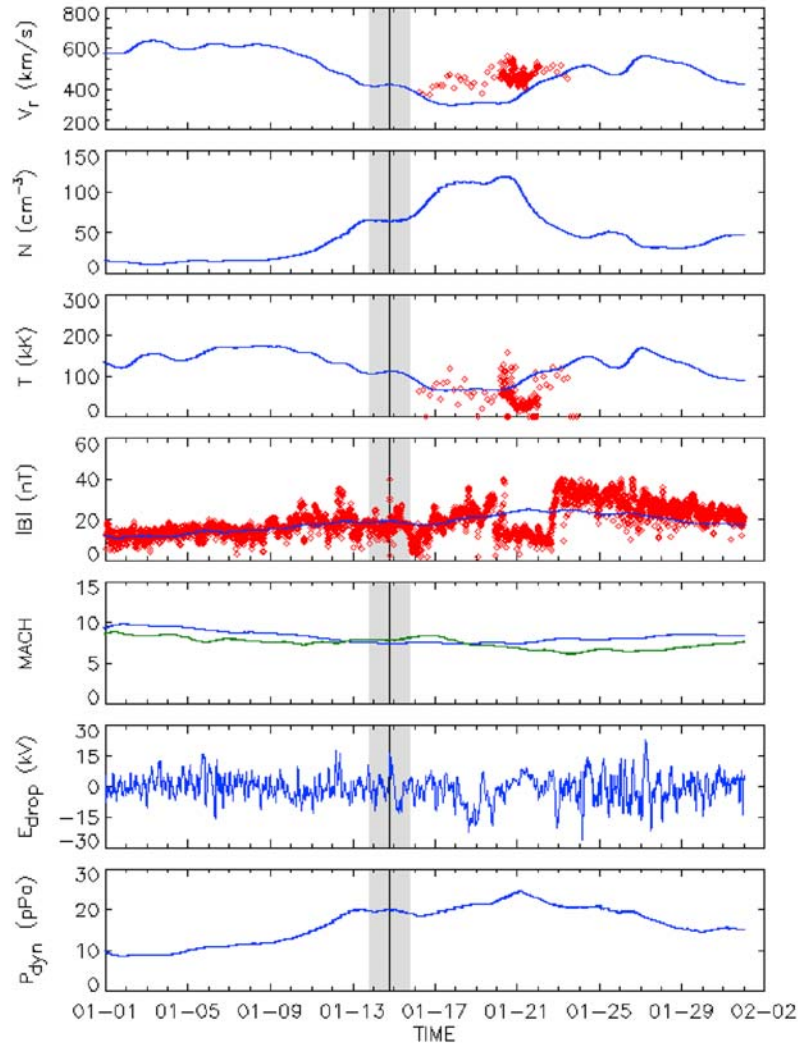


**Figure 6.** Computed SW parameters for January 2008. The shading in each panel shows the interval immediately surrounding the Mercury encounter period for MESSENGER (13–15 January). The first, second, and third panels show the SW speed, density, and temperature for this period, respectively (which matches the time period of Figures 3 and 4). The fourth panel shows the calculated value of the IMF magnitude for the same interval of time. The red data points plotted in the first, third, and fourth panels show MESSENGER magnetic field and available plasma data (as described in the text) for the period 1 January to 1 February 2008 for comparison. The bottom three panels show other (derived) quantities. The fifth panel shows the sonic and Alfvén Mach numbers. The sixth panel shows estimates of the cross-magnetospheric potential  $E_{\text{drop}}$  (see text), and the bottom panel shows dynamic pressure  $P_{\text{dyn}}$ .

As was the case for the ACE comparisons with the model output (Figure 3), WSA-ENLIL does a good job of forecasting the SW and IMF data both ahead and behind the Earth locations as seen by the STEREO-A and -B spacecraft comparisons.

[19] We note in Figures 3–5 that there are challenges in getting a proper comparison with the measured temperatures. For example, on STEREO the temperature plots are from an instrument that measures only protons (not electrons). Protons have higher temperatures than electrons (especially in fast streams from coronal holes). Numerical simulations provide the “mean” plasma temperature (which

by the above arguments, should therefore be lower than the plotted proton temperatures).

## 5. Comparison of Model Results With MESSENGER Data

[20] The SW temporal profiles and IMF parameter values that were calculated from the WSA-ENLIL model at the MESSENGER location from 1 January to 1 February 2008 are shown in Figure 6. From the model results, we see that the time of MESSENGER closest approach to the planet was, indeed, expected to be a period of relatively slow SW flow and relatively high density. The magnetic field strength

was computed to be gradually varying throughout this entire period, but the IMF was at a local plateau ( $B \sim 15$  nT) during the encounter period.

[21] In order to compare model results with the in situ spacecraft measurements, we plot the nearly continuous MESSENGER magnetometer data [Anderson *et al.*, 2008] on the model curve of  $B$  in Figure 6. These comparisons show that the model values are in good agreement with the measured values from MESSENGER throughout most of the month-long interval. An exception was for a brief period on 20–22 January, when the MESSENGER field magnitude dropped dramatically and model results were very different from the measurements. However, in broad terms, the ENLIL-MESSENGER magnetic field agreement was quite good.

[22] Because of the mounting position of the EPPS plasma analyzer [Zurbuchen *et al.*, 2008] on the spacecraft and because of spacecraft pointing constraints, we do not have continuous or complete MESSENGER measurements of the solar wind. During limited intervals throughout the period covered in Figure 6, however, the team was able to obtain a sufficient fraction of the distribution function to generate estimates of SW parameters (particularly speed and temperature). Data for such intervals are plotted in red on the respective model curves in Figure 6. The MESSENGER speed estimates are higher than the ENLIL calculations, but the inferred temperatures are low compared to the model. Naturally, the measured SW parameters show more structure and higher time variability than the model, which would be expected given the slower cadence of inputs (ground based) and inherent spatial smoothing to the model calculations. (Interestingly, most complete plasma measurements were derivable during the time of lowest and most disparate magnetic field values).

[23] The fifth, sixth, and seventh panels of Figure 6 provide derived parameters of considerable relevance (and utility) for magnetospheric modeling of the Mercury system. The fifth panel shows the sonic Mach number (in blue) and the Alfvén Mach number (in green). These values ( $<10$  throughout the encounter interval) are pertinent to estimating the expected bow shock and magnetopause properties at Mercury [Slavin *et al.*, 2008]. The sixth panel shows our calculated values of the potential drop  $E_{\text{drop}}$  (in kilovolts) across the Mercury magnetosphere. We have used the ENLIL model SW speed combined with the measured magnetic field normal component and a scaling distance of 1 Mercury radius ( $R_M = 2349$  km) to compute  $E_{\text{drop}}$ . Such potential drop estimates are an important aspect of the kinds of particle acceleration that might occur within the Mercury magnetotail [e.g., Baker *et al.*, 1986]. The seventh panel shows the SW dynamic pressure  $P_{\text{dyn}}$ .

## 6. Discussion and Future Work

[24] The combined WSA and ENLIL models provide contextual perspective on the SW and IMF conditions in the inner heliosphere during the time around the first MESSENGER flyby of Mercury. Our comparisons both before and after the time of closest approach show that the MESSENGER magnetometer measurements were in remarkably good agreement with model results for most of the 4-week-long interval of comparison. One relatively brief

period (20–22 January 2008) showed completely different magnetic field strengths than expected from the model predictions. Because of poor sensor placement, available MESSENGER SW measurements are of very limited utility for comparison with model outputs. The model results clearly show that Mercury’s magnetosphere on 14 January 2008 was being subjected to an extensive region of relatively low-speed, quiet SW. This information helps explain the benign, inactive magnetosphere that was sampled by MESSENGER sensors [Slavin *et al.*, 2008].

[25] The magnetic field data during the 20–22 January period showed a large reduction (generally) in the radial (from the Sun) component and also more fluctuations in the transverse components. As seen in Figure 6, the overall magnitude of the field was about half of the value expected from the model results. Since the MESSENGER plasma analyzer was also able to measure more of the SW plasma distribution during much of this interval (see Figure 6), we infer that the direction of SW flow must have been different (and more propitious for measuring its properties) during much of the anomalous magnetic field interval.

[26] We have looked at solar images and other remote sensing data for the period around 20 January 2008 to see if any features on the Sun might explain the weak field interval seen in the MESSENGER data. It is not obvious that any coronal or solar wind stream feature can be discerned. Thus, this aspect of the data-model comparison remains a puzzle.

[27] We assert that the present results are important in several respects. First, the methods utilized here can be used in a similar (or improved) fashion for future MESSENGER flybys of Mercury. Thus, we will be able to supply daily updated values of forecasted context information ( $\sim 1$ – $2$  days in advance at Mercury) for future in situ measurements. This will help in the prompt analysis and interpretation of flyby data and for the orbital phase of the MESSENGER mission. A second point is that the MESSENGER IMF (and any available SW) data in the inner heliosphere are quite useful local “ground truth” for the WSA-ENLIL model calculations. Having actual observations at  $\sim 0.3$ – $0.4$  AU heliocentric distance that can be “assimilated” into the model will help to improve and guide the overall model performance. In this sense, data-theory closure can lead to a better overall space weather prediction at Earth by the WSA-ENLIL combination [e.g., Baker *et al.*, 2004].

[28] As a final point, we can look forward to future measurements made of the Mercury system. For example, Earth-based measurements of the atmosphere of Mercury [e.g., Killen *et al.*, 2004] often would benefit from having a general knowledge of what type or intensity of SW is striking the planet (and its magnetosphere) at the time that ground telescopic data are acquired. The modeling shown here can help provide that useful contextual information. Beginning in 2011 when MESSENGER is in orbit around Mercury, the spacecraft will be within the magnetosphere and magnetotail of the planet for extended portions of each orbit. Model results will provide continuous information about the SW and IMF that is influencing magnetospheric dynamics and exospheric variability. We can also envision using the WSA-ENLIL time-dependent specifications and forecasts of SW parameters and IMF as inputs to many future magnetospheric simulation models [e.g., Kabin *et al.*, 2000].

[29] **Acknowledgments.** We thank two anonymous reviewers for helpful comments on an earlier version of this paper. The MESSENGER project is supported by the NASA Discovery Program under contracts NASW-00002 to the Carnegie Institution of Washington and NAS5-97271 to the Johns Hopkins University Applied Physics Laboratory. The work at CU Boulder was also supported by National Science Foundation Center for Integrated Space Weather Modeling (CISM).

[30] Wolfgang Baumjohann thanks the reviewers for their assistance in evaluating this paper.

## References

- Anderson, B. J., M. H. Acuña, H. Korth, M. E. Purucker, C. L. Johnson, J. A. Slavin, S. C. Solomon, and R. L. McNutt Jr. (2008), The structure of Mercury's magnetic field from MESSENGER's first flyby, *Science*, *321*, 82–85, doi:10.1126/science.1159081.
- Arge, C. N., and V. J. Pizzo (2000), Improvement in the prediction of SW conditions using near-real-time solar magnetic field updates, *J. Geophys. Res.*, *105*, 10,465–10,479, doi:10.1029/1999JA000262.
- Arge, C. N., J. G. Luhmann, D. Odstrcil, C. J. Shrijver, and Y. Li (2004), Stream structure and coronal sources of the solar wind during the May 12th, 1997 CME, *J. Atmos. Sol. Terr. Phys.*, *66*, 1295–1309, doi:10.1016/j.jastp.2004.03.018.
- Baker, D. N., J. A. Simpson, and J. H. Eraker (1986), A model of impulsive acceleration and transport of energetic particles in Mercury's magnetosphere, *J. Geophys. Res.*, *91*, 8742–8748, doi:10.1029/JA091iA08p08742.
- Baker, D. N., R. S. Weigel, E. J. Rigler, R. L. McPherron, D. Vassiliadis, C. N. Arge, G. L. Siscoe, and H. E. Spence (2004), Sun-to-magnetosphere modeling: CISM forecast model development using linked empirical methods, *J. Atmos. Sol. Terr. Phys.*, *66*, 1491–1497, doi:10.1016/j.jastp.2004.04.011.
- Kabin, K., T. I. Gombosi, D. L. Dezeew, and K. G. Powell (2000), Interaction of Mercury with the solar wind, *Icarus*, *143*, 397–406, doi:10.1006/icar.1999.6252.
- Killen, R. M., M. Sarantos, A. E. Potter, and P. Reiff (2004), Source rates and ion recycling rates for Na and K in Mercury's atmosphere, *Icarus*, *171*, 1–19, doi:10.1016/j.icarus.2004.04.007.
- McClintock, W. E., E. T. Bradley, R. J. Vervack Jr., R. M. Killen, A. L. Sprague, N. R. Izenberg, and S. C. Solomon (2008), Mercury's exosphere: Observations during MESSENGER's first Mercury flyby, *Science*, *321*, 92–94, doi:10.1126/science.1159467.
- Odstrcil, D., V. J. Pizzo, J. A. Linker, P. Riley, R. Lionello, and Z. Mikic (2004), Initial coupling of coronal and heliospheric numerical magnetohydrodynamic codes, *J. Atmos. Sol. Terr. Phys.*, *66*, 1311–1320, doi:10.1016/j.jastp.2004.04.007.
- Owens, M. J., C. N. Arge, H. E. Spence, and A. Pembroke (2005), An event-based approach to validating solar wind speed predictions: High speed enhancements in the Wang-Sheeley-Arge model, *J. Geophys. Res.*, *110*, A12105, doi:10.1029/2005JA011343.
- Russell, C. T., D. N. Baker, and J. A. Slavin (1988), The magnetosphere of Mercury, in *Mercury*, edited by F. Vilas, C. R. Chapman, and M. S. Matthews, pp. 514–561, Univ. of Ariz. Press, Tucson.
- Schatten, K. H., J. M. Wilcox, and N. F. Ness (1969), A model of interplanetary and coronal magnetic fields, *Sol. Phys.*, *6*, 442–455, doi:10.1007/BF00146478.
- Slavin, J. A., et al. (2008), Mercury's magnetosphere after MESSENGER's first flyby, *Science*, *321*, 85–89, doi:10.1126/science.1159040.
- Solomon, S. C., et al. (2008), Return to Mercury: A global perspective on MESSENGER's first Mercury flyby, *Science*, *321*, 59–62, doi:10.1126/science.1159706.
- Tóth, G., and D. Odstrcil (1996), Comparison of some flux corrected transport and total variation diminishing numerical schemes for hydrodynamic and magneto-hydrodynamic problems, *J. Comput. Phys.*, *128*, 82–100, doi:10.1006/jcph.1996.0197.
- Wang, Y.-M., and N. R. Sheeley Jr. (1992), On potential field models of the solar corona, *Astrophys. J.*, *392*, 310–319, doi:10.1086/171430.
- Zurbuchen, T. H., J. M. Raines, G. Gloeckler, S. M. Krimigis, J. A. Slavin, P. L. Koehn, R. M. Killen, A. L. Sprague, R. L. McNutt Jr., and S. C. Solomon (2008), MESSENGER observations of the composition of Mercury's ionized exosphere and plasma environment, *Science*, *321*, 90–92, doi:10.1126/science.1159314.
- B. J. Anderson, Johns Hopkins University Applied Physics Laboratory, 11100 Johns Hopkins Road, Laurel, MD 20723, USA.
- C. N. Arge, Air Force Research Laboratory, 3550 Aberdeen Avenue SE, Kirtland Air Force Base, NM 87117-5776, USA.
- D. N. Baker, Laboratory for Atmospheric and Space Physics, University of Colorado at Boulder, 1234 Innovation Drive, Boulder, CO 80309, USA. (daniel.baker@lasp.colorado.edu)
- M. Benna, Solar System Exploration Division, NASA Goddard Space Flight Center, 8800 Greenbelt Road, Greenbelt, MD 20771, USA.
- G. Gloeckler, J. M. Raines, and T. H. Zurbuchen, Department of Atmospheric, Oceanic and Space Sciences, University of Michigan, 2455 Hayward Street, Ann Arbor, MI 48109, USA.
- R. M. Killen, Department of Astronomy, University of Maryland, College Park, MD 20742, USA.
- D. Odstrcil, National Oceanic and Atmospheric Administration, 325 Broadway, Boulder, CO 80303, USA.
- D. Schriver, Institute for Geophysics and Planetary Physics, University of California, Slichter Hall Room 3871, Los Angeles, CA 90095, USA.
- J. A. Slavin, Heliophysics Science Division, NASA Goddard Space Flight Center, Mail Code 670, Greenbelt, MD 20771, USA.
- S. C. Solomon, Department of Terrestrial Magnetism, Carnegie Institution of Washington, 5241 Broad Branch Road NW, Washington, DC 20015, USA.